X-525-65-336

A SHORTENED HORN-REFLECTOR ANTENNA

SEPTEMBER 1965

GODDARD SPACE FLIGHT CENTER
GREENBELT, MARYLAND

X-525-65-336

A SHORTENED HORN-REFLECTOR ANTENNA

by

Paul A. Lantz

September 1965

Goddard Space Flight Center
Greenbelt, Maryland

CONTENTS

LIST OF ILLUSTRATIONS

A SHORTENED HORN-REFLECTOR ANTENNA

by

Paul A. Lantz

ABSTRACT

11221

A modification of a conventional horn reflector antenna is described in which the horn is replaced by a secondary hyperbolic subreflector, and Cassegrain feeding is used. Evolution of the geometric design is discussed. The aperture plane amplitude distribution is analyzed to compute the far-field pattern. Measured pattern and gain performance is presented and antenna temperature is estimated.

Author

A SHORTENED HORN-REFLECTOR ANTENNA

INTRODUCTION

The shortened horn-reflector antenna is a Cassegrainian adaption of a conventional horn reflector in which the horn is replaced by a hyperboloidal subreflector. This adaption overcomes the mechanical disadvantages and complexity of the conventional antenna and at the same time preserves its excellent electrical characteristics and does not require radome protection. This report describes the theoretical and experimental investigation of a 6-foot model designed for operation at 5.8 Gc. The investigation included an analysis of the reactive near-field region, the radiating near-field region, and the far-field region. Major effort was directed towards determining the aperture distribution in the reactive near field in order to utilize this information in determining the far-field pattern prior to experimental verification.

GEOMETRIC EVOLUTION

The geometric evolution of the shortened horn reflector can be described by initial reference to the geometry of the conventional horn reflector, Figure 1(a). Figure 1(a) shows that a parabolic curve is constructed with vertex at the origin 0 and with focal length OF = f. This curve is defined, in rectangular coordinates, by

$$y^2 = 4fx. \tag{1}$$

In deriving the horn-reflector geometry, it is easier to use polar coordinates in which case the parabola is defined by

$$r = \frac{2f}{1 + \sin \alpha}, \tag{2}$$

where α, the virtual source angle, is bounded by

$$-\alpha_0 \leq \alpha \leq \alpha_0 \tag{3}$$

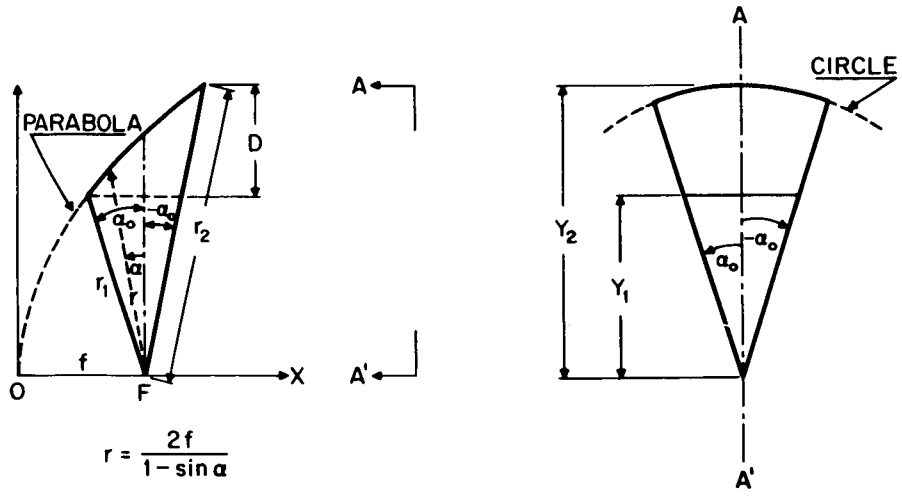

(a) CONVENTIONAL HORN REFLECTOR

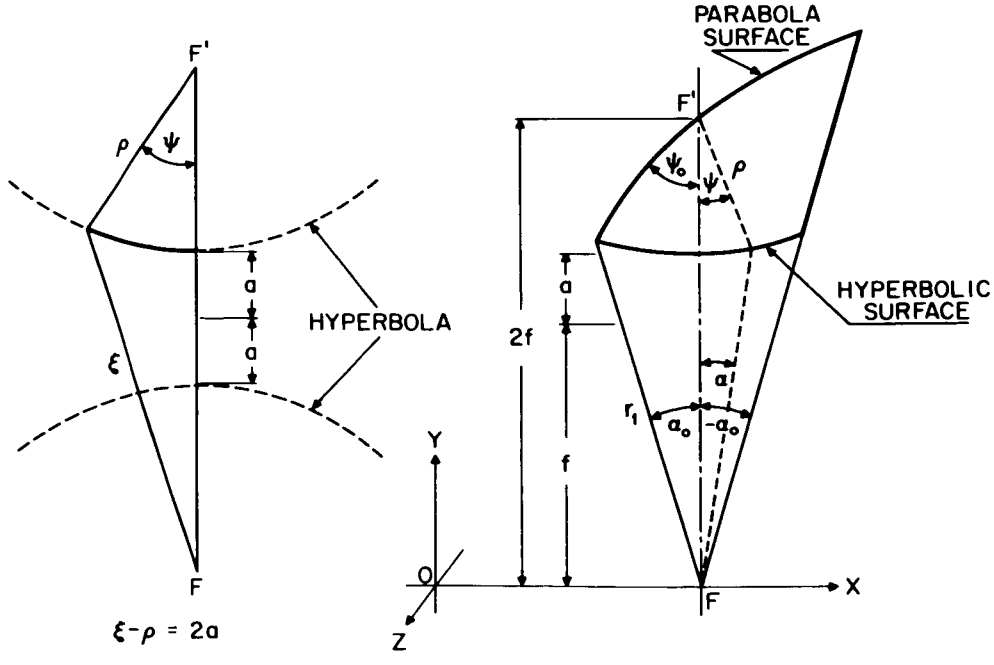

(b) HYPERBOLA GEOMETRY (c) SHORTENED HORN REFLECTOR

Figure 1–Geometric Evolution of Shortened Horn-Reflector Antenna

and α_0 and $-\alpha_0$ define the edge (flare angle) of the horn reflector. Rotation about the OX axis generates the paraboloidal reflecting surface.

Figure 1(a) shows that

$$D = y_2 - y_1, \tag{4}$$

and

$$y_1 = r_1 \cos(+\alpha_0)$$
$$y_2 = r_2 \cos(-\alpha_0). \tag{5}$$

Therefore

$$D = r_1 \cos(+\alpha_0) - r_2 \cos(-\alpha_0) \tag{6}$$

and

$$D = r_1 - r_2. \tag{7}$$

Since

$$r_1 = \frac{2f}{1 + \sin \alpha_0}$$
$$r_2 = \frac{2f}{1 - \sin \alpha_0} \tag{8}$$

therefore

$$D = \frac{2f}{1 + \sin \alpha_0} - \frac{2f}{1 - \sin \alpha_0} \tag{9}$$

and subtracting

$$D = 4f \tan \alpha_0. \tag{10}$$

The focal length of the paraboloidal reflector surface and the horn-flare angle thus define the aperture dimension.

The shortened horn reflector substitutes a hyperboloidal subreflector for the horn and employs Cassegrain feeding. A concave hyperbola with foci at F and F' is defined in Figure 1(b) by

$$\xi - \rho = 2a. \tag{11}$$

Figure 1(b) also shows that

$$\xi = [(\rho \sin \psi)^2 + (2f - \rho \cos \psi)^2]^{1/2} \tag{12}$$

which substituted in (11) yields,

$$\rho = \frac{f^2 - a^2}{a + f \cos \psi}. \tag{13}$$

Equation (13) represents a family of curves satisfying the focusing requirements. To define the hyperboloidal surface, "a" must be specified "a" in turn is dependent upon ψ_0 , the angle subtended by the hyperbola. The angle $2\psi_0$ is the feed angle. This consideration and a desire to minimize length dictate a hyperbola intersecting the parabola at the point established by a horn of flare angle α_0 . See Figure 1(c). From this figure

$$\tan \psi_0 = \frac{r_1 \sin \alpha_0}{2f - r_1 \cos \alpha_0}. \tag{14}$$

Substituting the value of r_1 given by equation (8),

$$\psi_0 = \tan^{-1}\left[\frac{\sin \alpha_0}{1 + \sin \alpha_0 - \cos \alpha_0}\right]. \tag{15}$$

At $\psi = \psi_0$, equation (11) becomes

$$2a = r_1 - \rho_1, \tag{16}$$

where r_1 is defined by equation (8), and from the geometry of Figure 1(c),

$$\rho_1 = \frac{r_1 \sin \alpha_0}{\sin \psi_0}. \tag{17}$$

Substitution of equations (8) and (17) in (16) yields,

$$a = \frac{f(\sin \psi_0 - \sin \alpha_0)}{\sin \psi_0 (1 + \sin \alpha_0)} \tag{18}$$

with ψ_0 defined in equation (15) as a function of α_0. The desired hyperboloidal reflecting surface is generated by rotation of FF′ of the hyperboloic section defined by equations (13), (15), and (18). Note that the complete design (i.e., the aperture size, the paraboloidal section, and the hyperboloid) is specified in terms of the paraboloidal focal length f and the flare angle α_0 of the equivalent horn section. Figure 2 shows the ratio a/f and the feed half angle ψ_0 as functions of α_0.

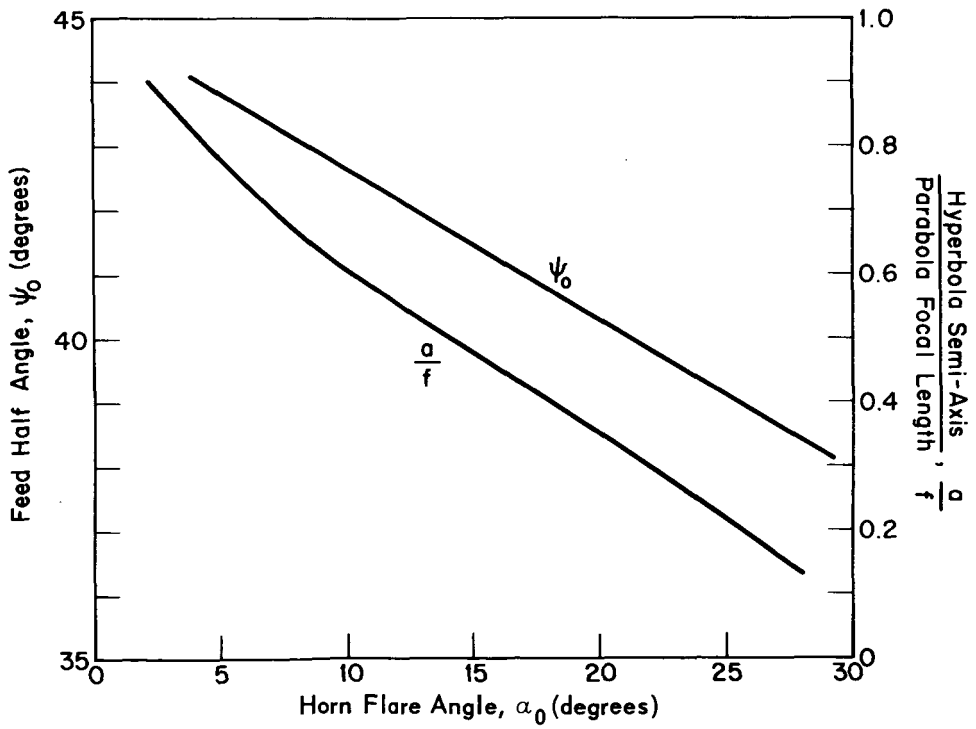

Figure 2-Design Parameter Relationship

Figure 3 shows a side view of the complete antenna. A typical ray is sketched as it emerges from the feed point, and is reflected from the hyperboloid and focused by the paraboloid. A difference in path length occurs for rays reflected from the extremities of the paraboloid. A symmetrical feed located at F' provides an assymmetrical amplitude distribution over the aperture plane as a result of this difference in path length. This space attenuation can be understood by reference to Figure 4, which illustrates the space taper geometry. Figure 4 shows two differential sections $\Delta\psi$ intercepting the edges of the hyperbola. Equal power flow is assumed through each section. The divergence of these equal power densities upon reflection to the parabola is easily determined considering that the equivalent horn of the conventional antenna exists (Figure 4). From the geometry, $\rho_1 \Delta\psi = r_1 \Delta\alpha_1$ and $\rho_2 \Delta\psi = \xi \Delta\alpha_2$. The space taper in db is

$$T_{(db)} = 20 \log \frac{r_1}{r_2} , \tag{19}$$

or in terms of the virtual source angle α_0 ,

$$T_{(db)} = 20 \log \left[\frac{1 - \sin \alpha_0}{1 + \sin \alpha_0}\right] . \tag{20}$$

Space taper for the design model in which $\alpha_0 = 15°$ is 4.6 db.

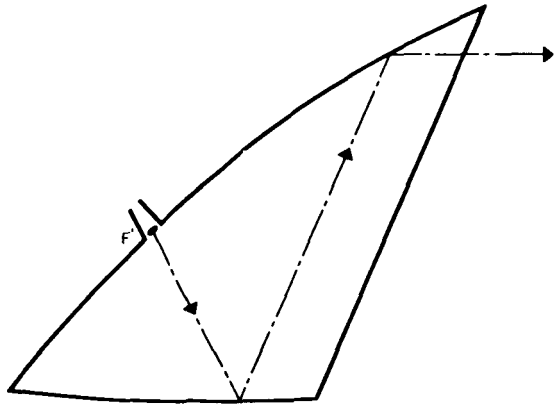

Figure 3–Typical Ray Trace, Shortened Horn Reflector Antenna

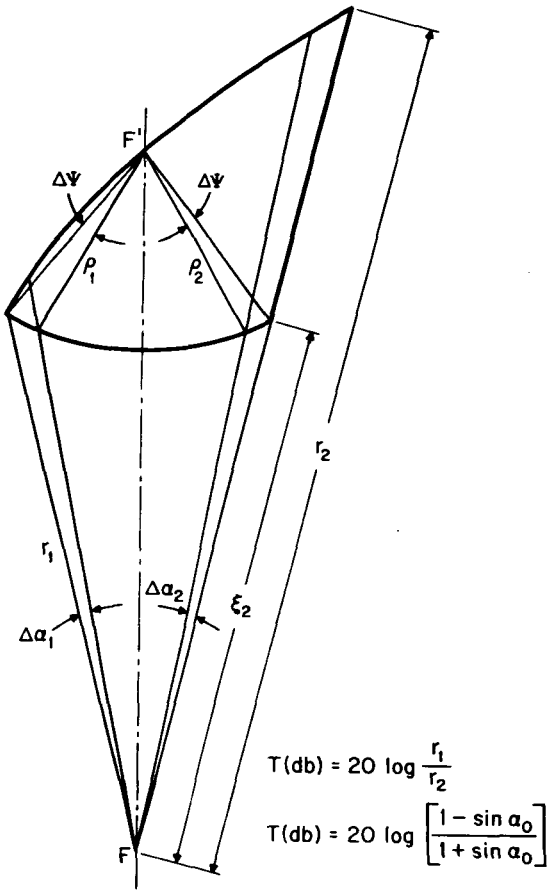

Figure 4–Geometry for Space Attenuation

APERTURE DISTRIBUTION

Evolution of the antenna proceeded along two parallel efforts: the theoretical analysis of RF properties, and experimental verification of findings. Three regions about an antenna are of interest: (1) the reactive near field, (2) the radiating near field (Fresnel zone), and (3) the far field (Fraunhofer zone).[1] It is the far-field performance which is of ultimate interest; however, it is the relationship between far-field performance and reactive near field (aperture distribution) which enables design optimization. Therefore, a careful study of aperture distribution was made. The nomenclature "transverse" aperture distribution and "longitudinal" aperture distribution was used as established by Bell Telephone Laboratories,[2] and is illustrated graphically in Figure 5.

---

[1]Hansen, R.C., "Microwave Scanning Antennas I", Vol. I, p. 29, Academic Press, 1964

[2]Crawford, A. B. et. al, "A Horn Reflector Antenna For Space Communication", BSTJ Vol XL, No. 4, July 1961, pp. 1095–1116

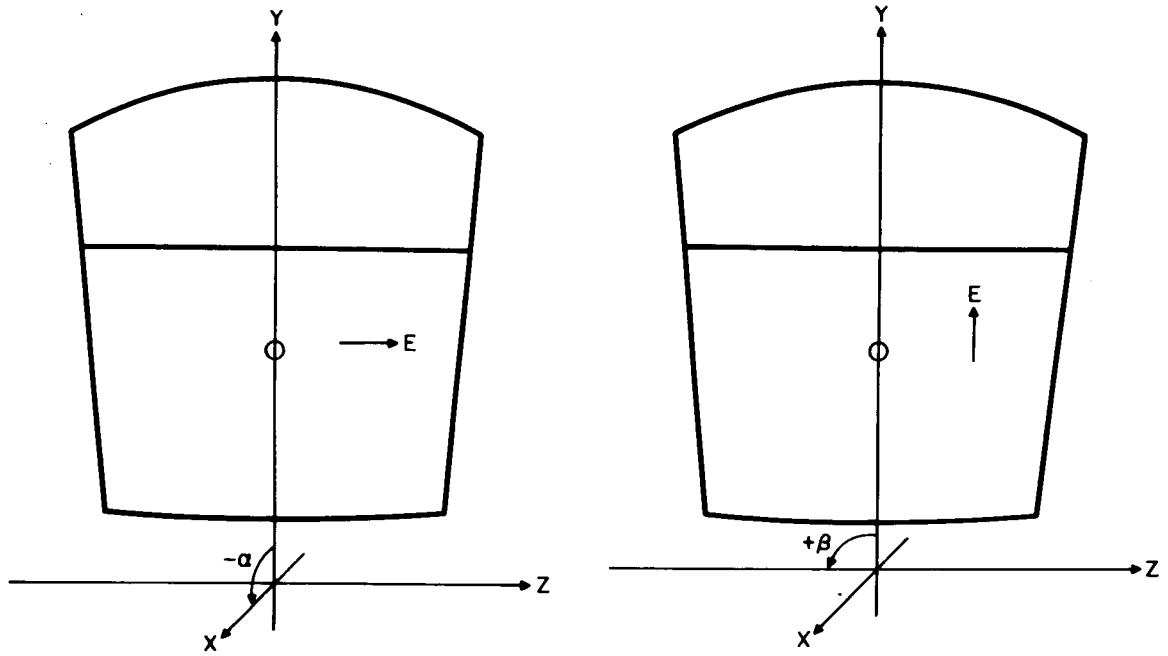

Figure 5–Polarization Nomenclature

If a field over a plane aperture is uniformly polarized, in the x-direction for example (the aperture being in the XY-plane), the field over the aperture can be designated as $F(\xi, \eta)$ where (ξ, η, o) is the point in the aperture plane from which energy emerges to a space point $P_{(x, y, z)}$. If $A(\xi, \eta)$ is the amplitude distribution, at the aperture point, and $\psi(\xi, \eta)$ is the phase distribution, then

$$F(\xi, \eta) = A(\xi, \eta)\, e^{-j\psi(\xi, \eta)}. \tag{21}$$

If $\vec{r}$ and $\vec{s}$ are unit vectors in the direction from the aperture point (ξ, η) to the field point P, then the far-field diffraction U_p is (Silver[3])

$$U_p = \frac{1}{4\pi} \int_A F(\xi, \eta)\, \frac{e^{-jkr}}{r} \left[\left(jk + \frac{1}{r} \right) \vec{i}_z \cdot \vec{r}_1 + jk\vec{i}_z \cdot \vec{s} \right] d\xi\, d\eta, \tag{22}$$

where k is the freespace propagation constant $2\pi/\lambda$. A number of simplifying approximations can be applied to this integral. The integral has a very valuable property, the Fourier transformation property, which makes it possible to compute the far-field pattern, U_p, from the aperture distribution $F(\xi, \eta)$. The

[3]Silver, S., "Microwave Antenna Theory and Design", McGraw-Hill, 1st ed. 1949, Chap. 6, pp. 169–199

primary effort of this program consisted of computing, and measuring, the aperture distribution and performing the Fourier transformation to obtain the far-field pattern.

The amplitude distribution across the antenna aperture was computed and measured with excellent agreement. These distributions were obtained using a rectangular waveguide horn with E- and H-plane aperture dimensions of 1.38 and 1.62 inches, respectively. The horn pattern had a 10-db taper at ±15 degrees. Figure 6 is a plot of the longitudinal plane aperture distribution measured along the horn centerline where $Z_n = 0$. (See the coordinate system on Figure 5.)

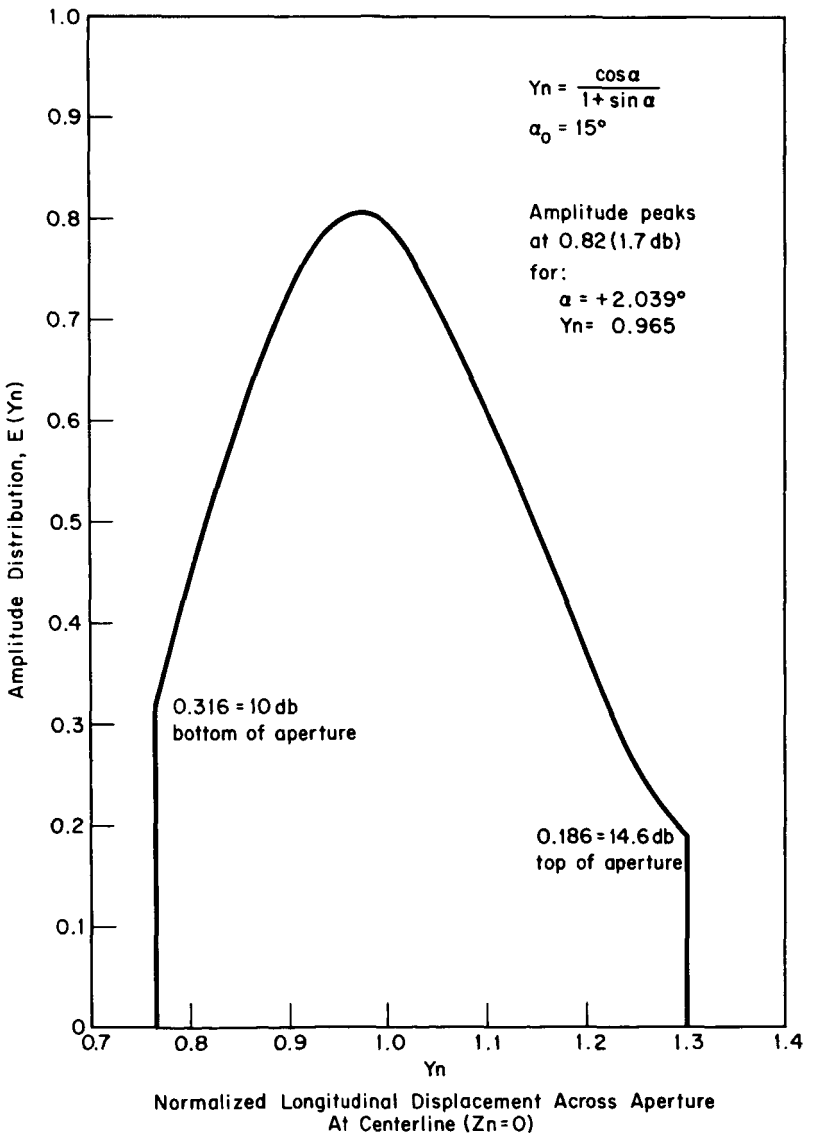

Figure 6–Longitudinal Plane Amplitude Distribution

Illumination at the lower edge of the aperture was observed to be 10 db, and at the top of the aperture 14.6 db, for the resultant $\cos^2$ on a pedestal distribution. The amplitude did not peak at $Y_n = 1.0$ (where $\alpha = 0$) but at $Y_n = 0.82$. Note that for values of $Y_n > 1$, α is negative and for values of $Y_n < 1$, α is positive. Peak illumination is down 0.82 (or 1.7 db) due to space attenuation of the horn signal. The assymetrical edge illumination is also a result of variation in space attenuation. Transverse plane aperture distribution is shown in Figure 7 where illumination at the edge of the aperture is shown to be down 12.5 db on each edge.

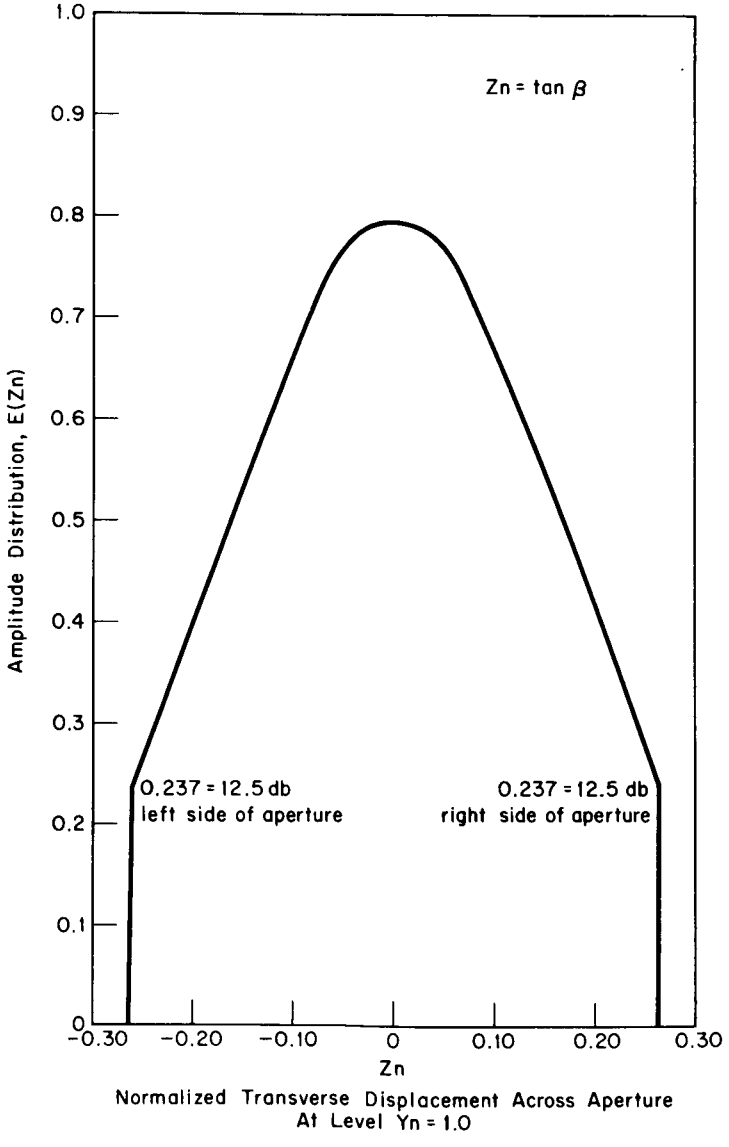

Figure 7–Transverse Plane Amplitude Distribution

The ordinate is displacement across the aperture in the Z plane at the level $Y_n = 1$. For this reason, the amplitude peak is only 0.79 (2.0 db) and not equal to the 1.7 db peak of the longitudinal plane distribution, which peaks slightly below $Y_n = 1$. Although a Fourier integral computer was not available at the time to calculate the far-field patterns of an aperture with these characteristics, the distribution could be accurately approximated by the sum of uniform, rectilinear, cosine, and sine distributions. Ramsay[4] has published Fourier transformations of these distributions and, by means of vector addition, excellent agreement was achieved between computed and measured far-field patterns. A newly acquired automatic Fourier integral computer is now being applied to recomputation of these patterns.

PATTERN PERFORMANCE

Figures 8 and 9 are computed far-field patterns for a frequency of 5.8 Gc. The 3-db beamwidth for the longitudinal plane is 1.74 degrees and sidelobes are predicted to be below 20 db. In the transverse plane, the 3-db beamwidth is shown to be 1.77 degrees and sidelobes are predicted to be below 26 db. Figure 10 is a composite display of calculated performance parameters plotted as a function of the virtual source angle, α. The choice of $\alpha = 15°$ was not the best choice because the illumination taper (difference in illumination between top and bottom edges of the aperture) across the aperture is excessive. Reduction of virtual source angle, to reduce illumination taper, causes an increase in sidelobe level. It is concluded from Figure 10 that a virtual source angle of $\alpha = 7.5°$ would be an optimum choice and an experimental model with 6-foot aperture dimension was built to this design. Feeding with a diagonal horn which illuminated the reflector edges with 11 db at 5.8 Gc produced the far-field patterns shown in Figures 11 and 12. Pattern performance is excellent. No sidelobes occurred above the isotropic level beyond ±20 degrees. Nonlinear pattern plots, measured with a crystal detector, indicated sidelobe level to continue to decay monotonically down to 60 db. A slight shoulder in the longitudinal plane pattern at 18 db is attributed to improper focusing of the feed horn which was optimized for transverse plane focus. Beamwidth compared nearly identically with calculated expectations, Figures 8 and 9.

APERTURE EFFICIENCY

Antenna efficiency is plotted in Figure 13 which shows that efficiency was 66 percent for the 11-db edge illumination used. This is to be compared to an

[4]Ramsay, J. F., "Fourier Transforms In Aerial Theory", Marconi Review, Vol. 9, No. 4, Oct–Dec 1946, pp. 139–145; Vol. 10, No. 1, Jan–Mar 1947, pp. 17–22

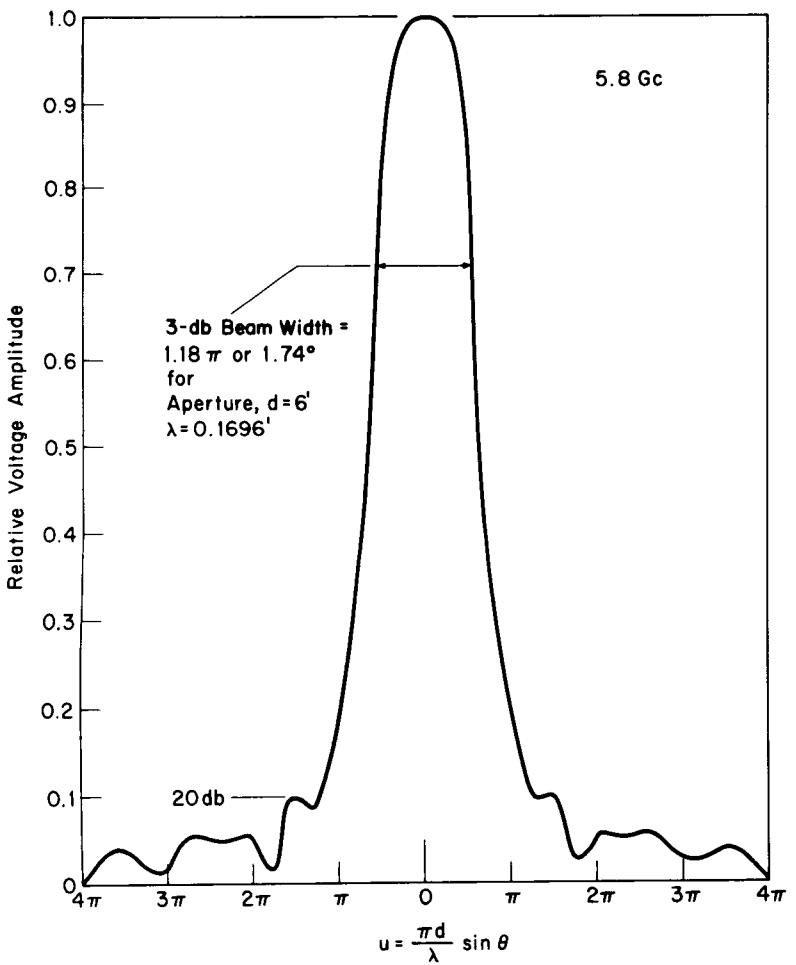

Figure 8–Computed Longitudinal Plane Pattern

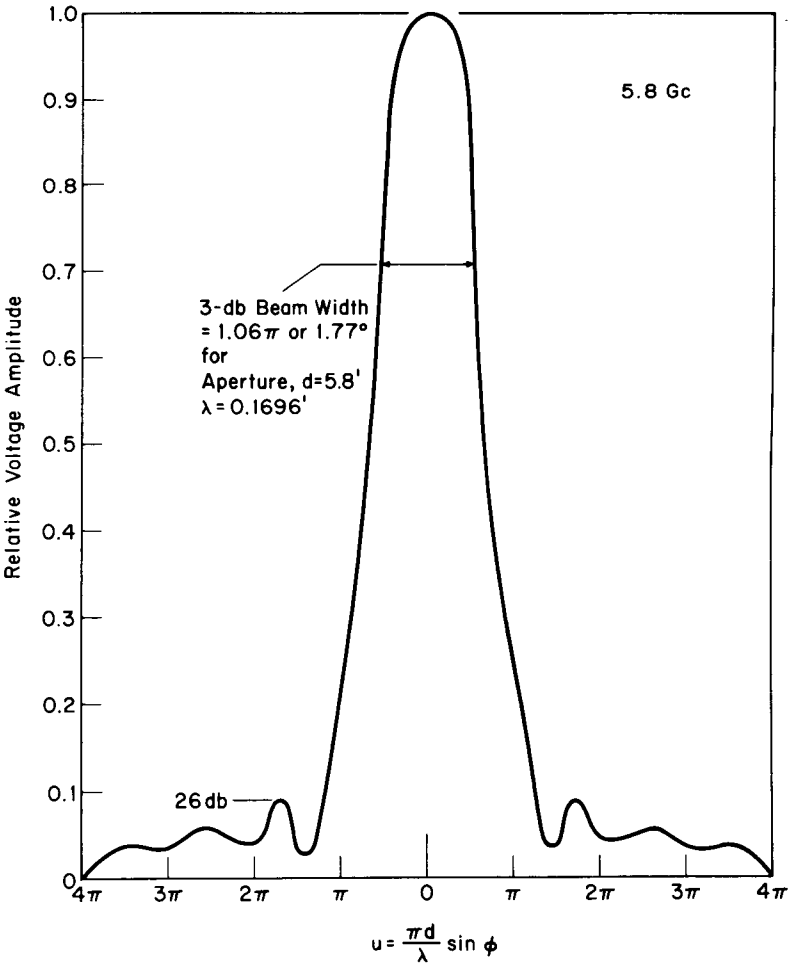

Figure 9–Computed Transverse Plane Pattern

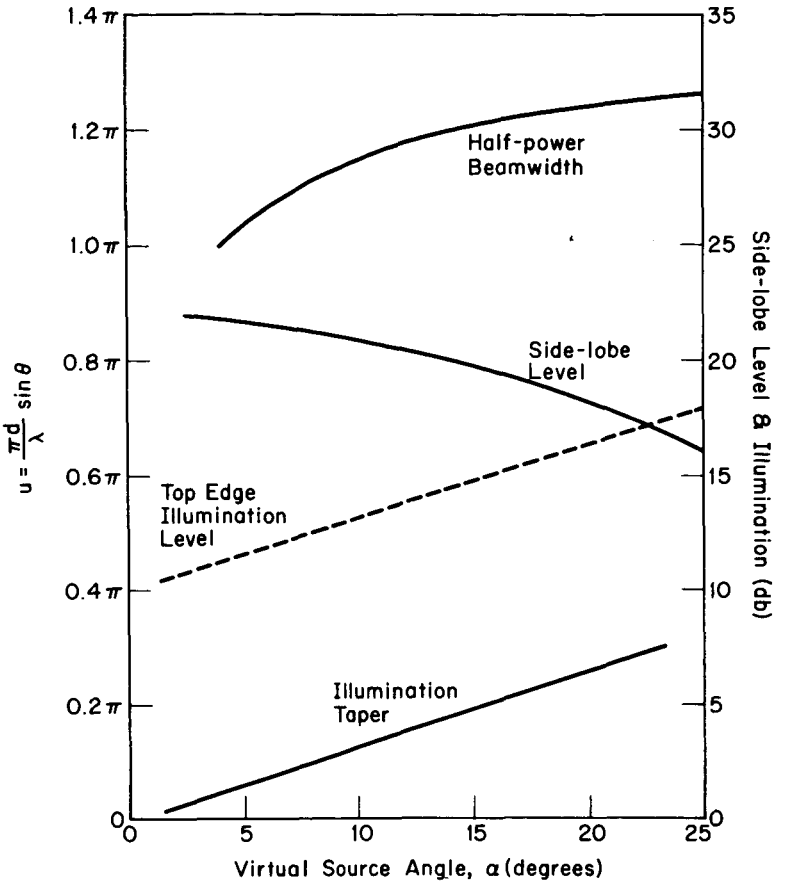

Figure 10–Calculated Longitudinal Plane Performance

efficiency of 55 percent with the conventional horn reflector. Antenna gain was measured to be 39 db at 5.8 Gc which Figures 11 and 12 show as the isotropic level.

ANTENNA TEMPERATURE

Antenna temperature was determined by integration of

$$T_a = \frac{1}{4\pi} \int_{\Omega} G(\theta, \phi) \; T(\theta, \phi) \, d\Omega \qquad (23)$$

where $G(\theta, \phi)$ is the gain of spatial coordinates measured at the antenna feed-horn terminal and $T(\theta, \phi)$ is the temperature distribution expressed in degrees

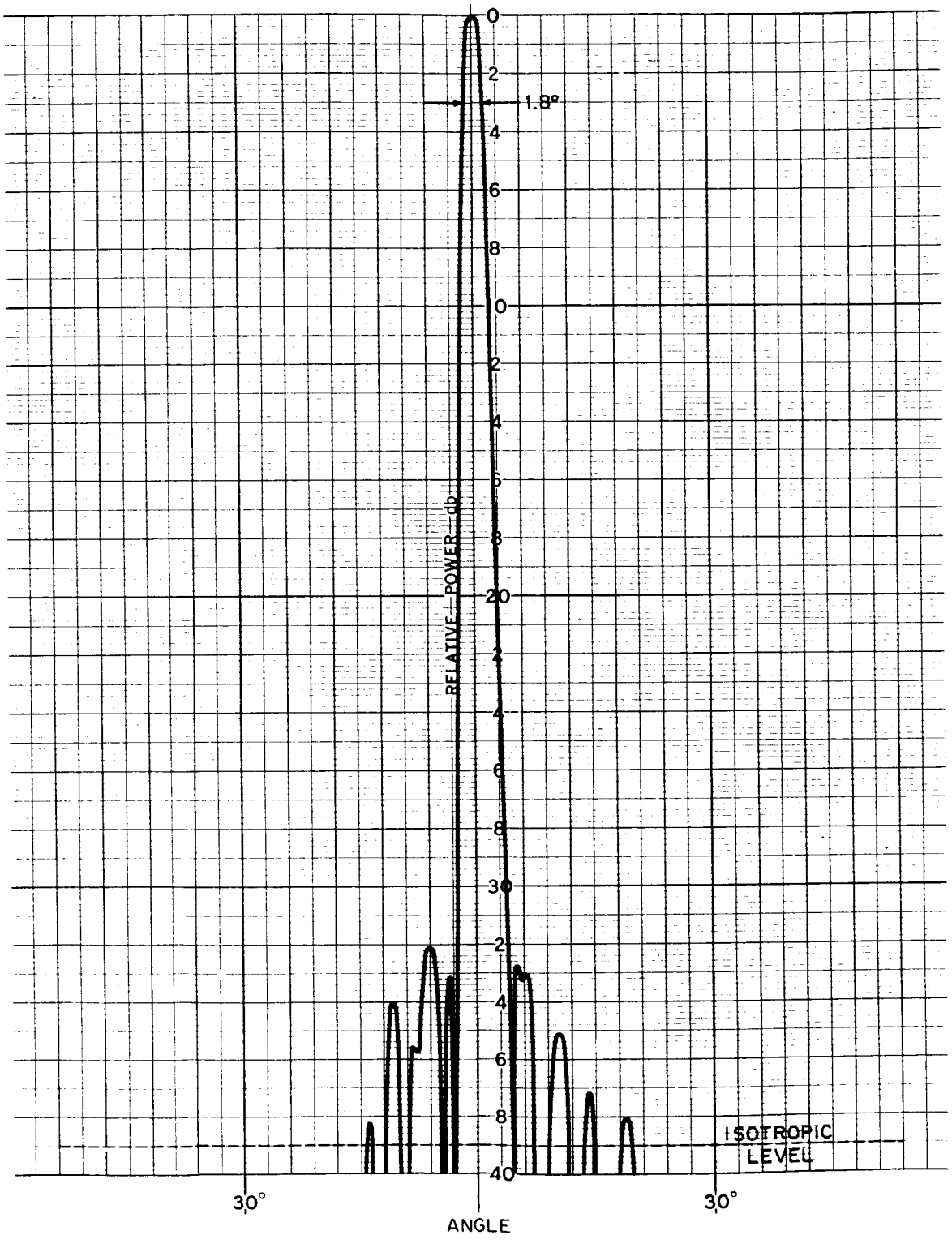

Figure 11–Measured Transverse Plane Pattern, 5.8 Gc

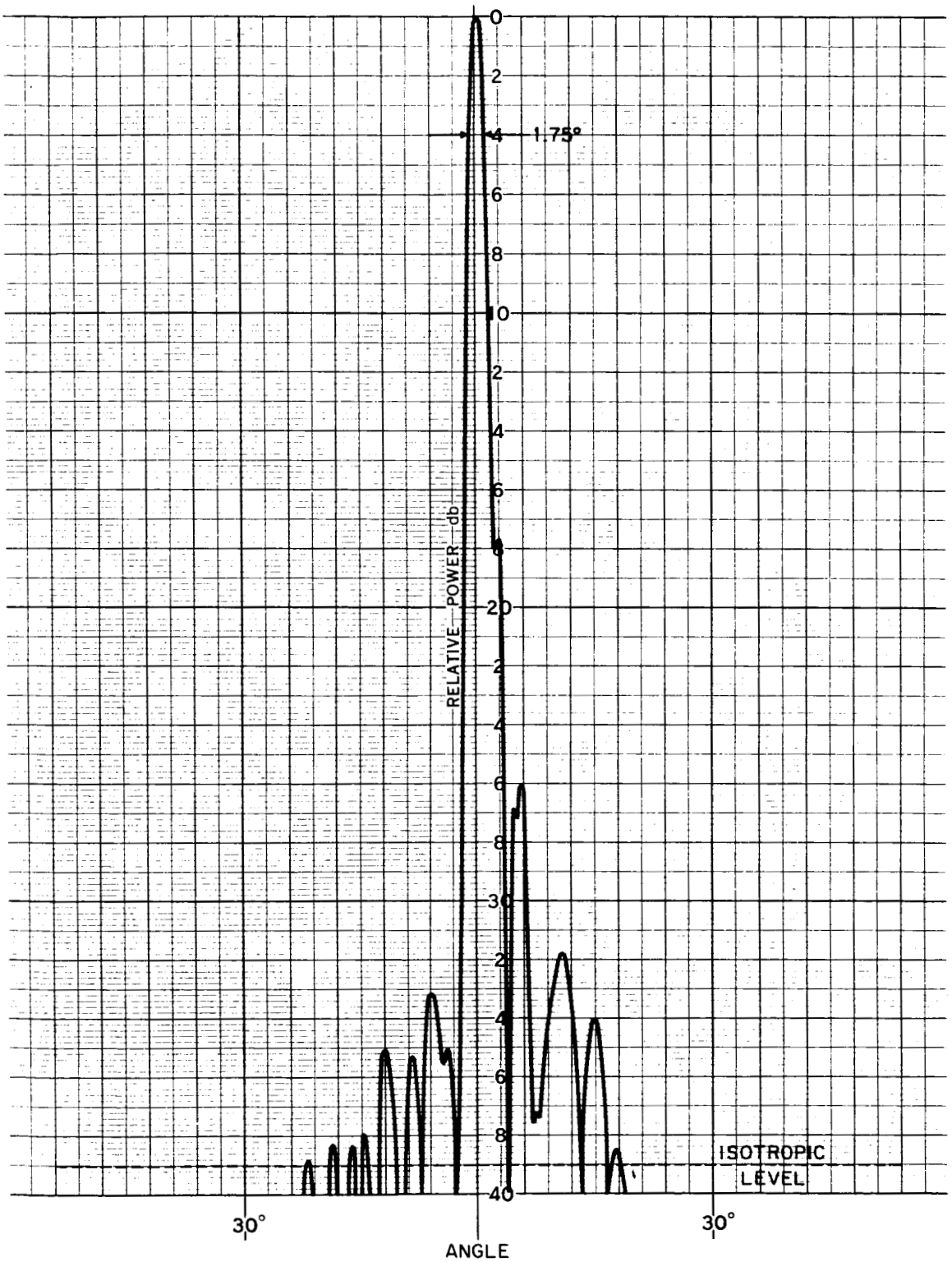

Figure 12–Measured Longitudinal Plane Pattern, 5.8 Gc

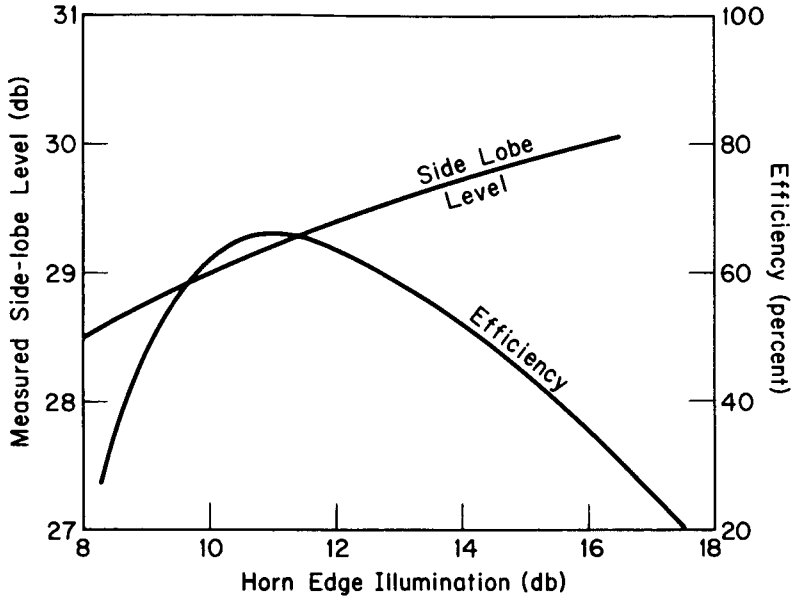

Figure 13-Performance Characteristics

Kelvin. This integration was performed over all space, and a temperature of 6°K for the 6-foot-antenna model was derived. This excellent performance makes the antenna especially suitable for space data acquisition. A monopulse feed was installed in the antenna to obtain a rough picture of performance in this application. Figure 14 shows the measured sum and difference patterns. Although no attempt was made to optimize monopulse performance, the patterns are very good, with sidelobes below isotropic beyond ±72 degrees.

CONCLUSION

The shortened horn-reflector antenna is an innovation in antenna design which offers broadband performance, economic construction, very low antenna temperature, and excellent pattern performance. A model, having a 6-foot aperture, was constructed demonstrating the rugged construction possibilities. Theoretical and measured performance analysis of this model enabled comparison to be made with a conventional horn reflector. Assuming both antennas are operated with a receiver having a temperature of 25°K, at C-band frequencies, and with feed line losses of 0.20 db, the following performance comparison can be made.

	Shortened Horn Reflector	Conventional Horn Reflector
Aperture efficiency	65%	55%
Antenna temperature	6°K	40°K
Figure of merit	1.7 db	-1.46 db

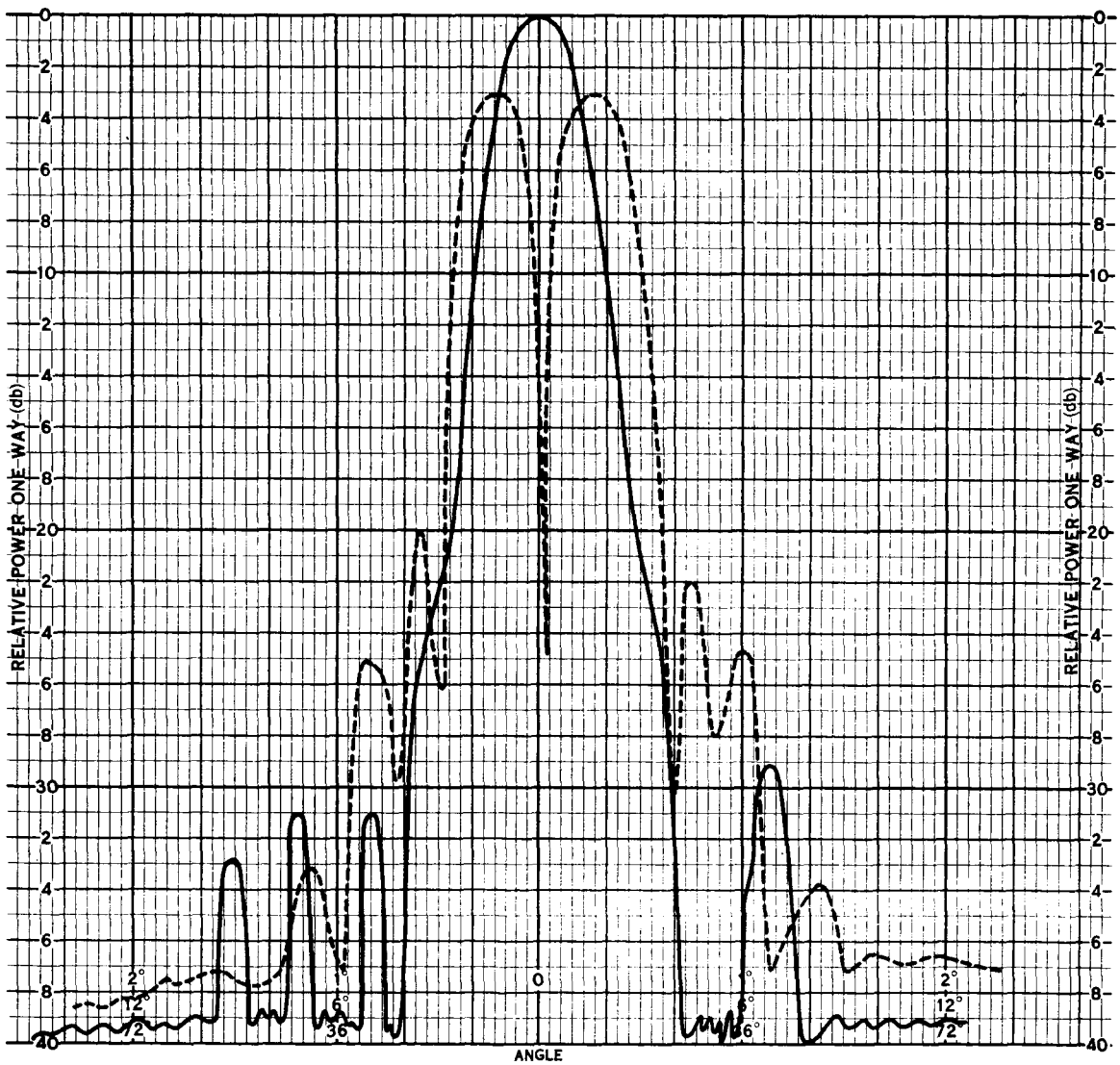

Figure 14–Measured Transverse Plane Sum and Difference Monopulse Patterns, 5.8 Gc